

PHLEGRA MONTES, MARS: CHRONOLOGY AND DENUDATION RATES

S. van Gasselt¹, A.-P. Rossi², C. Orge^{1,3}, J. Schulz¹. ¹Freie Universität Berlin, Department of Earth Sciences, D-12249 Berlin, Germany (Stephan.vanGasselt@fu-berlin.de); ²Jacobs University Bremen, Earth and Space Sciences, D-28759 Bremen, Germany; ³Eötvös Loránd University, Department of Geology, Budapest, 1053 Hungary.

Background: The Phlegra Montes are located north-east of the Elysium rise (165°E, 29.5–51.0°N) and form a 1,250 km long topographically well-pronounced arcuate ridge composed of Hesperian to Noachian-aged remnant massifs [1] with associated debris aprons and lineated valley fill features (fig. 1). Considered to be of endogenic tectonic origin in earlier work [2], the Phlegra Montes have recently been interpreted as unit composed of degraded Hesperian-aged ($3.65_{0.06}^{0.04}$ Gyr (eHt) and $3.71_{0.10}^{0.06}$ Gyr (IHt)), and Noachian- to Hesperian-aged ($3.77_{0.07}^{0.05}$ – $3.91_{0.18}^{0.08}$ Gyr HNt) material of potentially volcanic origin pre-dating the Hesperian plains-forming lowland material [1]. Younger mass-wasting material covering these remnants is considered to be of Hesperian age [1].

The Phlegra Montes cover more than twenty degrees in latitude and form a complex system of isolated hills, ridges and small basins that provide insight into large climate-controlled geomorphologic settings and processes on Mars. The Phlegra Montes form a longitudinally confined traverse through climatic zones that are known to host features indicative of ground ice and/or even glacial ice [3, 4]. Despite such value, the region has received little attention and has been revisited only relatively recently when radar-data interpretations provided new arguments in favour of extensive glaciation [5, 6, 7], and local geomorphologic studies provided reasons to believe that the region was once covered by extensive ice sheets [8, 9] several hundred Myr ago. Our study is concentrated on a systematic survey covering detailed age distributions of surface units as function of latitude in order (a) to obtain statistically representative and latitudinally dependent age estimates—in particular as there are discrepancies with respect to the youthfulness of local surface-ages [9, 1]. Furthermore, the survey is carried out (b) to derive upper denudation-rate estimates for mass-wasting units under the assumption of hyper-arid climate conditions favouring periglacial denudation. We expect that latitudinal trends will potentially be observable within the limits of accuracy of morphometric measurements and age determinations if young-Amazonian climate variations control formation of icy aprons on Mars.

Approach and Analysis: Data analysis is based on high-resolution image data obtained by the MRO Context Imager (CTX) [10] and MGS Mars Observer Camera (MOC) [11] instruments and is complemented by med- to high-resolution context images from the MEX High Resolution Stereo Camera (HRSC) [12, 13] and the

MO THEMIS (VIS/IR) instruments [14]. Topography is derived using (a) gridded MGS Mars Orbiter Laser Altimeter (MOLA) data [15, 16], (b) photogrammetrically-derived stereo information from HRSC [17, 18] (absolute and regional scales) and (c) photoclinometrically-derived information using observation- and illumination-geometries (relative and local scales).

Our primary aim is the systematic assessment of representative surface ages using impact-crater size-frequency statistics with recent chronology models and definition of the Martian impact-crater production function described in [19]. Crater-based age determinations are based on areas that we considered as geologically distinct and homogeneous, and that were formed by a distinct process. Diameter-sizes are determined using the ArcGIS *CraterTools* extension by [20]. Analysis of impact-crater size-frequency statistics and derivation of model ages were carried out using *Craterstats II* [21] using recently summarised, updated and refined methodological approaches described by [22, 19, 23]. Data on systematic age determinations are supplemented by selected morphometric

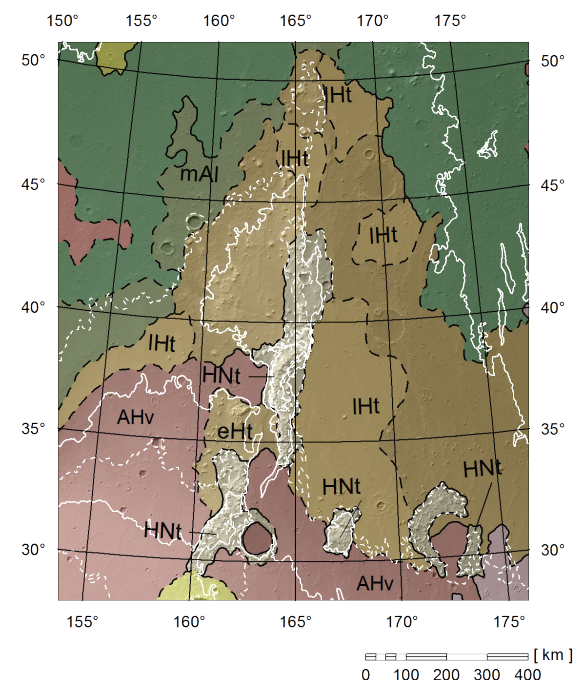


Figure 1: Hillshade topography (MOLA) and geologic units as published by [1]. Generalized contours are in dashed (500 m) and solid white lines (1000 m) based on MOLA GDR [16].

measurements in order to estimate denudation ages and rates, according to the methodological framework described in [24], allowing comparison with rover-based estimates [25, 26]. However, rates are difficult to assess owing to considerable uncertainties regarding the formation age of remnant massifs and limited knowledge and data on extents of aprons.

Results: Ages have been measured for 36 areas over the study region (fig. 2). Ages of volcanic units in the south are comparable to recent published measurements and are in the range of $3.43_{0.57}^{0.12}$ Gyr to $3.54_{0.19}^{0.07}$ Gyr after resurfacing correction. A younger signal might refer to

new resurfacing events, e.g. new volcanic emplacements as subdued impact crater suggest. It remains noteworthy that resurfacing has been a continuing process indicated by flattened crater-size frequency distributions. Significant resurfacing events took place around $2.09_{0.19}^{0.19}$ for the southern basin unit and at $1.06_{0.17}^{0.17}$ Gyr for intra-ridge units. Lineated valley fill areas in the central study region (fig. 2) show several age signals, as old as 3.5 Gyr for the underlying terrain and as young as 71 Myr for youngest surface (comparable to previously published ages).

Measurements of denudation rates of aprons across the overall study area indicate values of $0.01\text{--}0.02 \text{ mm} \pm 10^{-3} \text{ mm a}^{-1}$ since the Hesperian–Noachian transition which is – partially due to relief – at least one order of magnitude higher than conventional estimates for areas on Mars, e.g., [26]. It is conceivable that high rates indicate an interplay of (a) atmospheric deposition of ice and flow (glacial context), and (b) denudation of hillslopes and gravitational creep of ice and debris (periglacial context).

Acknowledgement: This work is partially supported by the National Space Administration with means of the Federal Ministry for Economic Affairs and Energy (grant 50QM1301).

References: [1] K. L. Tanaka et al. 2014. *U.S. Geol. Surv. Sci. Inv. Map.* 3292. [2] J. M. Moore. 1985. *Lun. Planet. Sci. Conf. Abs.*, XVI: 573–574. [3] M. H. Carr & G. G. Schaber. 1977. *J. Geophys. Res.*, **82**(28): 4,039–4,054. [4] S. W. Squyres. 1979. *J. Geophys. Res.*, **84**(B14): 8,087–8,096. [5] A. Safaeinili et al. 2009. *Lun. Planet. Sci. Conf. Abs.*, XL: #1988. [6] J. W. Holt et al. 2008. *Science*, **322**(5905): 1235–1238. [7] J. J. Plaut et al. 2009. *Geophys. Res. Lett.*, **36**(2): L02203. [8] A. Kress et al. 2010. *Lun. Planet. Sci. Conf. Abs.*, XLI: #1166 [9] J. L. Dickson et al. 2010. *Earth Planet Sci. Lett.*, **294**(3–4): 332–342. [10] M. C. Malin et al. 2007. *J. Geophys. Res.*, **112**, E05S04. [11] M. C. Malin et al. 1992. *J. Geophys. Res.*, **97**(E5): 7,699–7,718. [12] G. Neukum et al. 2004. *ESA–Spec. Pub.*, **1240**: 17–35. [13] R. Jaumann et al. 2007. *Planet. Space Sci.*, **55**(7–8): 928–952. [14] P. R. Christensen et al. 2004. *Space Sci. Rev.*, **110**(1): 85–130. [15] D. E. Smith et al. 2001. *J. Geophys. Res.*, **106**(E10): 23,689–23,722. [16] D. E. Smith et al. 2003. NASA PDS, MGS–M–MOLA–5–MEGDR–L3–V1.0 [17] F. Scholten et al. 2005. *Photogram. Eng. & Rem. Sens.*, **71**(10): 1,143–1,152. [18] K. Gwinner et al. 2010. *Earth Planet. Sci. Lett.*, **294**(3–4): 506–519. [19] G. G. Michael 2013. *Icarus*, **226**(1): 885–890. [20] T. Kneissl et al. 2011. *Planet. Space Sci.*, **59**(11–12): 1,243–1,254. [21] G. G. Michael & G. Neukum 2010. *Earth Planet. Sci. Lett.*, **294**(3–4): 223–229. [22] G. G. Michael et al. 2012. *Icarus*, **218**(1): 169–177. [23] T. Platz et al. 2013. *Icarus*, **225**(1): 806–827. [24] S. van Gasselt et al. 2011. *Geol. Soc. London Spec. Pub.*, **356**: 43–67. [25] M. P. Golombek et al. 2006. *J. Geophys. Res.*, **111**(E12). [26] M. H. Carr 1992. *Proc. 23rd Annual Lun. Planet. Sci. Conf.* 205–206.

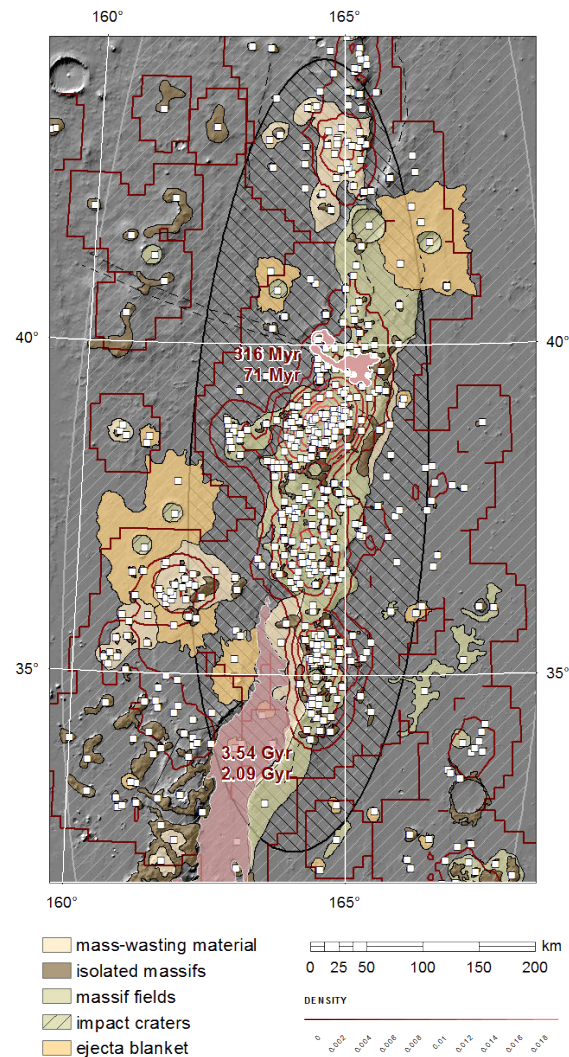


Figure 2: Main geomorphic and geologic units superimposed by remnant distribution (white boxes + density plot in red and $1\text{-}\sigma$ distribution (hachured)). Two selected areas with associated age measurements are marked in bright red.